PORE MORPHOLOGY VARIATION UNDER AMBIENT CURING OF PLAIN AND FIBER-REINFORCED HIGH PERFORMANCE MORTAR AT AN EARLY AGE

Jesús Mínguez[1,*], Miguel A. Vicente[1,2], Dorys C. González[1,2].

[1] Department of Civil Engineering, University of Burgos. c/Villadiego, s/n. 09001. Burgos. Spain.

[2] Parks College of Engineering, Aviation & Technology, Saint Louis University, 3450 Lindell Blvd, 63103 Saint. Louis, MO. USA

[*] Corresponding Author. Tel: +34 947 259 523. E-mail: jminguez@ubu.es

Keywords: pore morphology, plain mortar, fiber reinforced mortar, CT-Scan technology.

ABSTRACT

Pore morphology and its changes at an early age in two different mortar mixtures are analyzed by means of a CT-Scan and DIP software. Both mixtures share the same cement paste composition. The only difference between them is the inclusion of 0.1% by volume of steel fibers in one paste and its omission from the other paste. A total of six specimen cylinders measuring 45.2 mm in diameter and 50 mm in height were cast. All the specimens were held in a controlled atmosphere at 20ºC and at 60% humidity, reflecting natural ambient curing conditions. Each specimen was scanned at 1, 2, 3, 4, and 7 days using a micro CT-Scan. The data were analyzed using a digital image processin (DIP) software and some post-processing subroutines. Each individual void was identified and isolated and all its geometrical parameters were measured. Among the most interesting and relevant findings was that the presence of fibers substantially modified the pore morphology, increasing the volume of voids, and the pore-size, and reducing the shape factor of the voids, among other effects. Both mixtures showed different pore morphologies at the beginning of the curing process that metamorphosed into different and even divergent geometrical dimensions.

1. INTRODUCTION

All concrete elements contain a certain percentage of voids, which differ greatly from one piece to another. In general, concrete porosity is residual and non-desirable. However, in other cases, concrete design entails the use of air-entrainment agents to have a specific percentage porosity.

The voids content has a strong influence on the macroscopic behavior of concrete at all ages. In case of fresh concrete, the content of voids modifies its rheology [1-3]. Thus, for example, an increase in the voids content results in a reduction of concrete viscosity, which is very important in case of pumpable concretes [4]. In case of hardened concrete, the voids content influences many aspects, such us permeability [5-7]. Another interesting case is pervious concrete, designed with a very high porosity, so that, among other applications, road surfaces can, even in heavy rain, remain relatively dry [5, 7].

The strong relation may also be highlighted between voids content and behavior under freeze-thaw cycles [8, 9]. In fact, concrete subjected to very intense freeze-thaw cycles must be designed with a minimum threshold of voids content. Additionally, the voids content also influences concrete behavior at high temperatures [10] and its behavior under cyclic loading, among other aspects [11-13].

Depending on the void size, they can be classified into micropores (smaller than 1 μm), mesopores (between 1 μm and 10 mm) and macropores, as well as macropores or simply pores (larger than 10 mm) [14]. Several methods are used to analyze voids. The traditional ones are nitrogen absorption and mercury-intrusion porosimetry (MIP) [15, 16]. These traditional methods show two main limitations. First, they can only provide pore-size distribution, but not the pore distribution, shape, etc. Second, these techniques can only provide information on open porosity, but not on closed porosity.

A novel technology has recently been successfully applied to concrete: computerized tomography (CT) scan technology. Beyond the use of CT scans in medicine, a lot of research has recently been conducted on the analysis of internal concrete microstructure. Most have focused on fiber-reinforced concrete and therefore on fiber orientation [12, 17, 18]. However, interest has, over the past few years, been focused on internal voids with several works published on the topic [4, 5, 19-26].

In case of fiber-reinforced concrete, fibers have a strong influence on the macroscopic behavior of concrete at all ages. Fibers are commonly used to improve the mechanical behavior of hardened concrete. For example, they are commonly used to reduce the cracking, which improves the durability of the structure [27, 28]. They are also used to improve fatigue life [29-31], to increase tensile strength [32, 33], and to improve behavior under freeze-thaw cycles [34, 35], among other uses.

The inclusion of fibers in fresh concrete modifies its behavior, by increasing concrete paste viscosity [36-40].

However, all the research mentioned above implicitly assume that fibers do not modify the concrete matrix. This work demonstrates that steel fibers significantly modify the voids content of concrete and its porosity. A fiber presence results in a different evolution of internal porosity during the early age of concrete and likewise in hardened concretes that reveals different patterns of internal voids. In recent years, some interesting research projects have been carried out to study the interfacial zone between the fibers and the cement paste, in order to analyze whether, at this level, a variation in the cement paste composition occurs. In all cases, the nano-indentation technique is used; usually combined with scanning electron microscopy (SEM) [41-43]. The results show differences in the composition of the cement paste in this zone, although its influence on the macroscopic behavior of the material has not been deeply studied.

Mortar is a particular case of concrete, where no coarse aggregate is used. All the issues described above are also applicable to mortar.

In this work, two different mortar mixtures have been studied: plain and steel fiber-reinforced mortar. The only difference between each is the inclusion or otherwise of fibers. All the specimens have been scanned using a CT-Scan to detect the voids. Using post-processing routines, especially developed by the authors, the pore morphology in both mixtures has been observed and compared: porosity, pore-size distribution, pore shape, etc. Additionally, the variation during the early age has been studied and a very different change has been detected.

The objective of this work is to analyze the change of the pore morphology and the main geometrical parameters of the voids of these two mortar mixtures over time during the first curing week, and how the presence of fibers modifies this change over time.

The structure of the paper is as follows: the experimental procedure is presented in Section 2; the results of the tests are described and discussed in Section 3; and finally, the conclusions are shared in Section 4.

2. EXPERIMENTAL PROGRAM

The materials, the manufacturing procedure and the scanning procedure are described in this section.

2.1 Materials

In this study, a total of six cylinders were cast. The specimen dimensions were 45.2 mm in diameter and 50 mm in height. Three of them were made of steel fiber-reinforced mortar (SFRM) and three of plain mortar (PM). Table 1 shows the mixture proportions.

Table 1: Mixture proportions

Materials	PM	SFRM
Cement (kg/m^3)	700.0	
Water (kg/m^3)	217.0	
Superplasticizer (kg/m^3)	24.5	
Nanosilica (kg/m^3)	10.5	
Fine aggregate (0/4) (kg/m^3)	1,400.0	
Fiber (% by volume)	0.0%	0.1%

An amount of 7.8 kg/m^3 of steel Dramix 8/.16 (BEKAERT, Kortrijk, Belgium), fiber were added to manufacture the fiber-reinforced mortar, resulting in a fiber volume fraction of 0.1%. The fibers measured 8 mm in length and 0.16 mm in diameter and had an aspect ratio of 29. According to the supplier information, the tensile strength was 3000 MPa and the modulus of elasticity was 200 GPa. The mortar mass included MasterRoc MS 685 (BASF, Ludwigshafen am Rhein, Germany) nanosilica, Glenium 52 (BASF, Ludwigshafen am Rhein, Germany) superplasticizer and siliceous aggregate, with a nominal maximum aggregate size of 4 mm that were all mixed with a high strength Portland cement CEM I 52.5 R.

It can be noticed in Table 1 that mortar has been considered in this work, instead of concrete. This is because the CT-Scan demands small-sized specimens to obtain accuracy enough to detect properly the voids. In this situation, the use of coarse aggregate in small specimens results in a high scatter between the different specimens, which complicate the further analysis. In addition, the dimensions of the specimen are chosen to assure a successful scanning process, with high accuracy.

Additionally, 2 prisms 40x40x160 mm were performed; one per mixture. A total of 3 cubes with 40 mm edges were obtained from each prism and tested under compression in order to characterize their compression strength (according to [44]). The average compressive strength f_c was 68.6 MPa for PM and 69.2 MPa for SFRM, with a standard deviation of 1.7 MPa and 1.9 MPa respectively. From a statistical point of view, no difference between PM and SFRM can be observed regarding compressive strength. The mean mortar density ρ was 2343 kg/m^3 and 2348 kg/m^3 for PM and SFRM respectively, with a standard deviation of 23.3 kg/m^3 and 23.5 kg/m^3 respectively. Again, from a statistical point of view, there is no difference between both mortars regarding density.

The viscosity of the fresh mortar was measured, for both mixtures, by flow table according to [45]. The results obtained were 240 mm for PM and 210 for SFRM. In both cases the mixtures can be considered as fluid, although PM show more flowability than SFRM.

2.2 Specimen manufacturing process

PVC molds with an inner diameter of 45.2 mm, an outer diameter of 50 mm and a height of 50 mm were used to cast the specimens. The PVC molds were built using a commercial PVC pipe. The base of each cast was a PVC disc with a diameter of 60 mm and a thickness of 3 mm. The base was welded to the pipes, in order to assure a watertight joint (Figure 1). The mortar was prepared in a cement mortar mixer, following the manufacturing specifications in standard EN 196-1:2016. The protocol of mixing was the same for the two mixtures. First, the dry components were poured on the mixer and finally the water and the superplasticizer were added. In case of the SFRM, finally, the fibers were added. The molds were filled in two parts using a small aluminum scoop to form the specimens without applying vibration. However, some small punches were applied on the side of the molds, once it was filled with mortar, to help mortar to expel the entrapped air. Finally, the upper surface was smoothed with a trowel. Once cast, all the specimens were held under controlled conditions at 20ºC and 60% humidity, reflecting ambient curing conditions more closely than a conventional curing room, where specimens remain at 20ºC and 100% humidity.

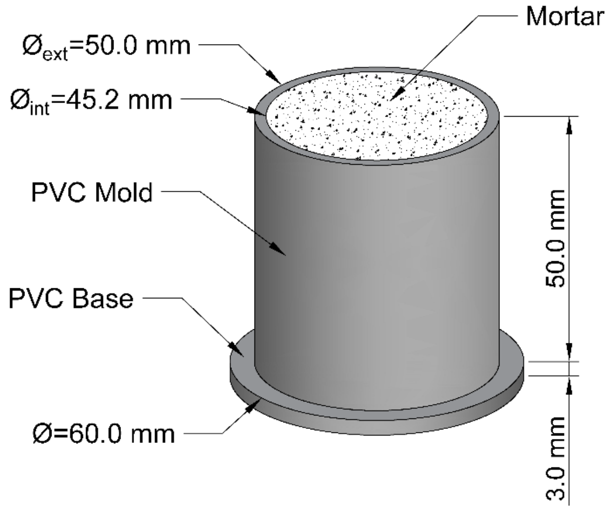

Figure 1: Specimen and mold

2.3 Scanning process

This study is focused on the behavior of mortar during an early age, in particular during the first week of curing where the most relevant changes in the microstructure of mortar are expected to occur. To do so, all the specimens were scanned daily on the 1st, 2nd, 3rd, 4th and 7th day, using a micro-CT Scan.

A GE Phoenix v|tome|x CT system equipped with a 300 kV/500W nano-focus x-ray tube was used at the '*Centro Nacional de Investigación sobre la Evolución Humana (CENIEH)*', (Burgos, Spain). The accelerating voltage was 160 kV and the current was 150 μA. The CT-Scan has post-processing software that generates 2D images with 2048x2048 pixels. Thus, the equipment provides a horizontal resolution of 25x25 μm^2 for a section with a diameter of 45.2 mm. The vertical distance between the cutting planes was fixed at 25 μm, so the CT-Scan produced 2,000 images per specimen, such as those shown in Figures 2 and 3. The voxel size was 25x25x25 μm^3. The post-processing software created a 3D image of the specimens using all of the above-mentioned images. The software assigns a grey level to each voxel (volumetric pixel), varying from 0 to 255 (where 0 is equal to black and 255 is equal to white), depending on the real density of the matter at that point. Light grey voxels correspond to denser points and dark grey ones, to less dense ones, i.e., voids. The output of all this process was a matrix that included the X, Y, and Z coordinates of the voxel center of gravity and a number, from 0 to 255, referring to the density. The total number of voxels in each specimen were approximately $4.3\cdot10^9$.

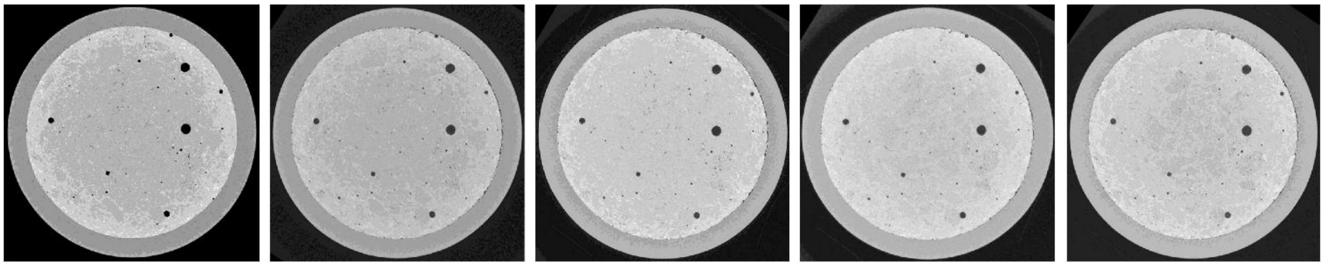

Figure 2: Slices belonging to plain mortar at different ages. From left to right: 1, 2, 3, 4 and 7-days age.

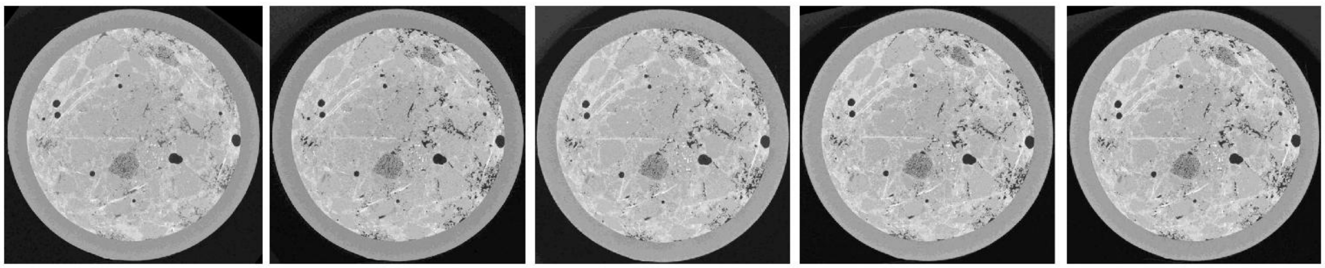

Figure 3: Slices belonging to steel fiber-reinforced mortar at different ages. From left to right: 1, 2, 3, 4 and 7-days age.

The Digital Image Processing (DIP) software AVIZO (FEI Visualization Sciences Group, Hillsboro, Oregon, USA) was then used to identify and isolate each individual void inside the specimen. Firstly, the software identified the voxels showing a grey below a certain threshold. In this case, having studied the histogram of grey distribution, the threshold of 65 was considered (Figure 4).

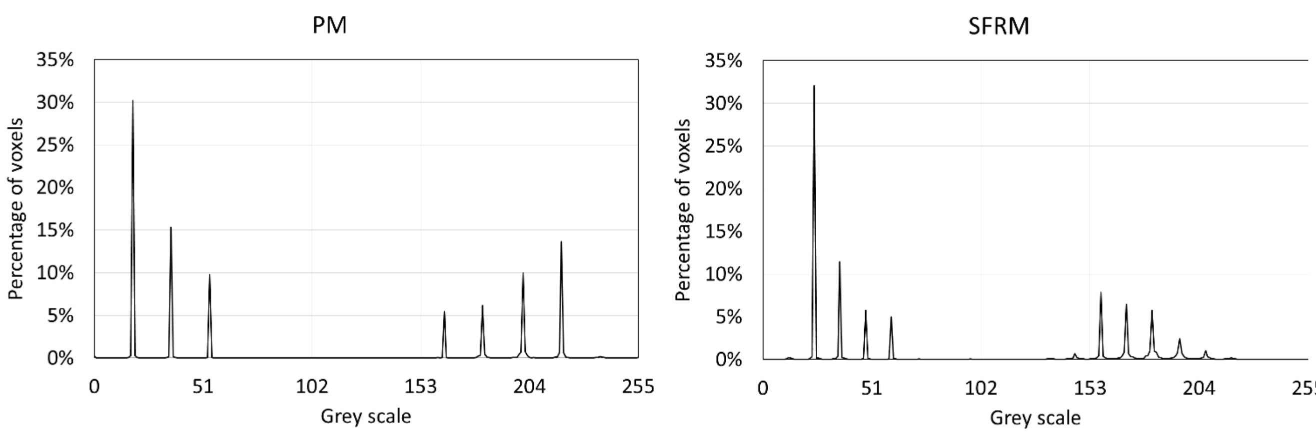

Figure 4: Histograms of grey distribution.

Figure 4 shows that there is a high percentage of voids below 65, which means empty voxels. However, not all of them belongs to voids, most of them are placed in the empty space placed outside the mold. So, the next step was to delete all the voxels which do not belong to the mortar specimen, i.e., the ones placed outside the inner face of the mold. The vertical axis of the specimen at each slice is first defined. Next, all the pixels with a distance to the center of the specimen greater than the radius of the specimen are removed. Moreover, the histograms of Figure 4 cannot be used to obtain the percentage of voids in the specimen.

Next, all the voxels in contact with each other were grouped, as they represented to the same void. The software identified and isolated the different voids and the final result of the scanning was a dot matrix containing the Cartesian coordinates X, Y and Z of the center of gravity of the pore. Figures 5 and 6 show the image of one specimen of each mixture over time.

Figure 5: 3D views belonging to plain mortar at different ages. From left to right: 1, 2, 3, 4 and 7-days age.

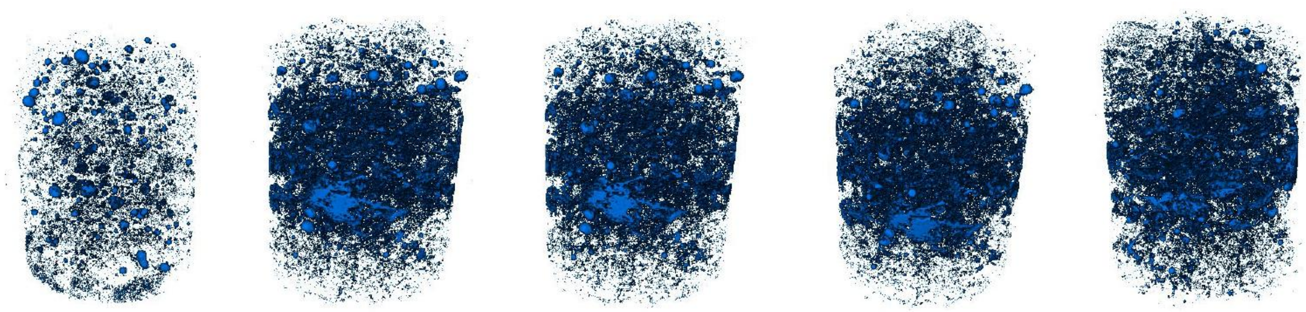

Figure 6: 3D views belonging to steel fiber-reinforced mortar at different ages. From left to right: 1, 2, 3, 4 and 7-days age.

The first finding of this work is that a relevant number of macropores are placed on the lateral border of the specimen, in contact with the mold, which can be explained by certain phenomena. Firstly, the mortar specimens show a wall effect, leading to a greater percentage of the smallest particles of mortar (water, cement and filler) on the lateral border. Slight mortar shrinkage leads to a gap between mortar and mold, a space that is initially filled with water and then by air. However these “pores” are not the same as voids and may distort the results.

Therefore, the lateral region of each specimen was removed, so that instead of the whole specimen, only the inner core of the specimen was analyzed, i.e. a cylinder with a diameter that was 90% of the real diameter of the specimen, i.e., 40.7 mm and the whole height. Additionally, two slices were discarded in both top and bottom faces in order to prevent erroneous results at the very top and bottom ends. In consequence, the studied height was 49.9 mm (Figure 7).

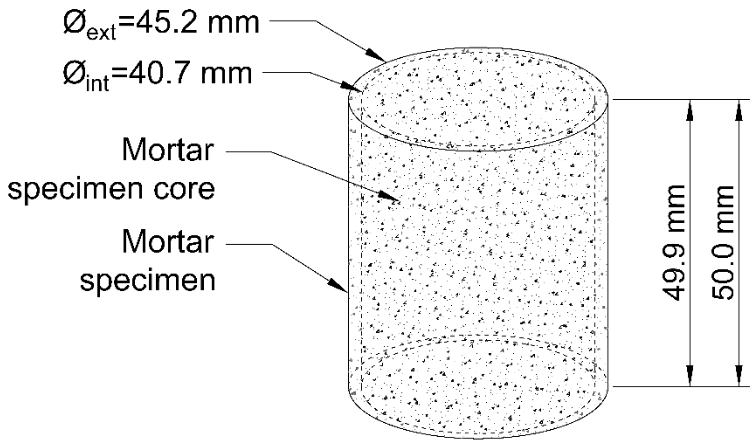

Figure 7: Portion of the mortar to be studied

In this work, voids with a less than 3 voxels in the largest direction (i.e., 75 μm length approximately) were discarded as too small. Moreover, they were not sharply enough defined in the CT-Scan for clear identification. Additionally, pores larger than 10 mm in the largest direction were discarded as non-representative pores.

In consequence, all the micropores [14] are discarded, since they are not possible to be detected using this technology, and also the smaller portion of the mesopores. In addition, the macropores are also discarded since they represent an extremely low percentage of the total amount of voids (in all cases less than 8 voids have been detected, which represents less than 0.01% of the total amount of voids) and a big scatter between the specimens is observed (a difference of 1 void between one specimen and other represents a huge difference in relative terms). In consequence, macropores do not provide useful information.

3. RESULTS AND DISCUSSION

A visual inspection of the 3D images is unable to detect relevant differences in the internal porosity between the specimens nor how they evolve at early ages. The use of DIP software in combination with customized post-processing routines was required, for a deep analysis of the data and to extract the relevant information. The results from the post-processing stage are presented in this Section. The values shown in the different tables and figures refer to the average values of the three specimens belonging to the same mixture. In all cases it has been observed that the coefficient of variation (COV) is below 10%, which means that the specimens show a low scatter.

3.1 Total volume of voids and porosity

The first two parameters to be studied in this research are the total volume of voids and the porosity. This last parameter is defined as the ratio between the total volume of voids and the volume of the specimen considered in this study (i.e. a cylinder with a diameter of 40.7 mm and a height of 49.9 mm, as explained in Section 2).

Both parameters were obtained on the 5 different days when the measurements took place over the first week, as mentioned in Section 2 (i.e., 1, 2, 3, 4 and 7 days). Figure 8 shows the changes of the pore volume and the porosity of both mixtures with the age.

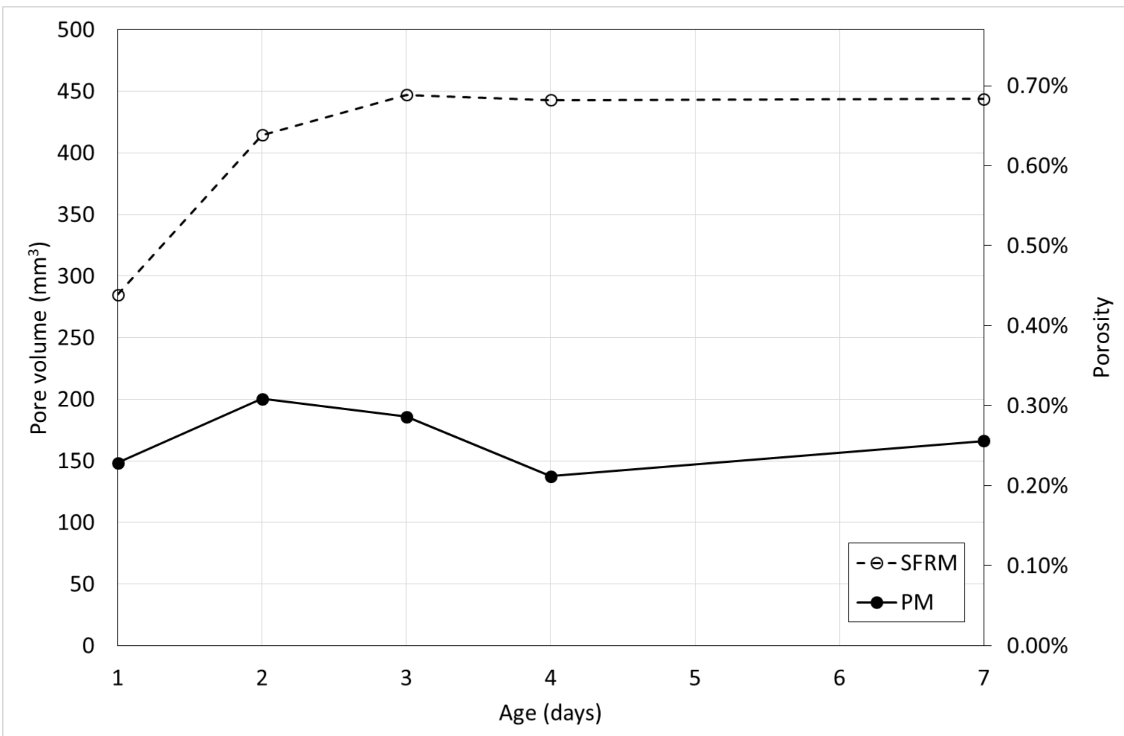

Figure 8: Change of the total volume of voids and the porosity over time of mortar

The voids inside the specimens can be due to entrapped air and due to the initial water drops than then become voids (since the water is consumed during the hydration process and/or is evaporated).

Some interesting conclusions can be obtained from Figure 8. The first and most striking conclusion was that the total volume of voids and the porosity was greater in the steel fiber-reinforced mortar (SFRM) than in plain mortar (PM). Since the specimens were no vibrated, a relevant percentage of the voids are because of entrapped air, which tend to be greater than the ones because of initial water drops transformed into voids. These results demonstrate that the presence of fibers results in an increase of the voids content, i.e., the fibers increases the entrapped air.

They also agree with the results obtained by other researchers [45, 47], who observed that the presence of polypropylene fibers increased the viscosity of the fresh mortar, hindering the removal of entrained air and inducing greater porosity.

Regarding the changes in porosity over time, it can be seen that SFRM showed a progressive increase in porosity over time, although it was a damped process. On the contrary, the PM specimens showed no relevant changes over time. The SFRM specimens showed greater porosity than the PM specimens at the beginning of the hardening process (first day). Over the first three days there was a global increase of porosity in both mixtures, although it was more relevant in case of SFRM. Then, the porosity of the PM decreased on the 4th day, following which a slight increase was observed. In case of the SFRM, the porosity remained almost constant after the 3rd day.

The dynamic nature of the voids content with two different mechanisms acting in opposing directions was clearly observable. The first one, the hydration process, is a water-consuming activity. At the beginning of the hydration process almost all the voids were full of water and a minimum amount of air was left inside the mortar matrix. As the density of voids full of water is not very different from the one shown by fresh mortar paste, they could not be distinguished in the CT-Scan. Over time and due to the consumption of water during the cement hydration process, the voids empty and dry out, leaving the spaces to be filled by air, which makes them “visible” in the CT-Scan. The curing process therefore results in a progressive increase of the voids content and the porosity of the mortar mixture.

On the contrary, the air entrapped inside the voids tends to rise and eventually leave the mortar specimen. In addition, the spaces tend to be occupied by the fresh cement paste, i.e., the voids tend to collapse. This second phenomenon implies a progressive decrease of the void content and the porosity of the mortar mixtures. Macroscopically, the consequence are the autogenous shrinkage and the drying shrinkage.

The SFRM specimens, because of the presence of fibers, showed a more consistent mortar matrix than the PM specimens. In consequence, the first phenomenon described above prevailed over the second one, resulting in an overall increase of the voids content and porosity over time. On the contrary, the PM showed a fresh and less consistent mortar matrix with both properties equally balanced. In consequence, the void content and the porosity remained almost constant over time [37].

3.2 Variation of the total porosity along the depth

Using the coordinates of the center of gravity of each individual void, and more specifically its Z coordinate, it is possible to establish the changes of the voids content and the porosity throughout the depth. Figure 9 shows the change in porosity throughout the depth by the age of the mortar, in both mixtures. In all cases, the depth is shown in relative terms, i.e., varying from 0 to 1 where 0 refers to the free surface of the specimens and 1 refers to the other end of the specimens, i.e., the bottom.

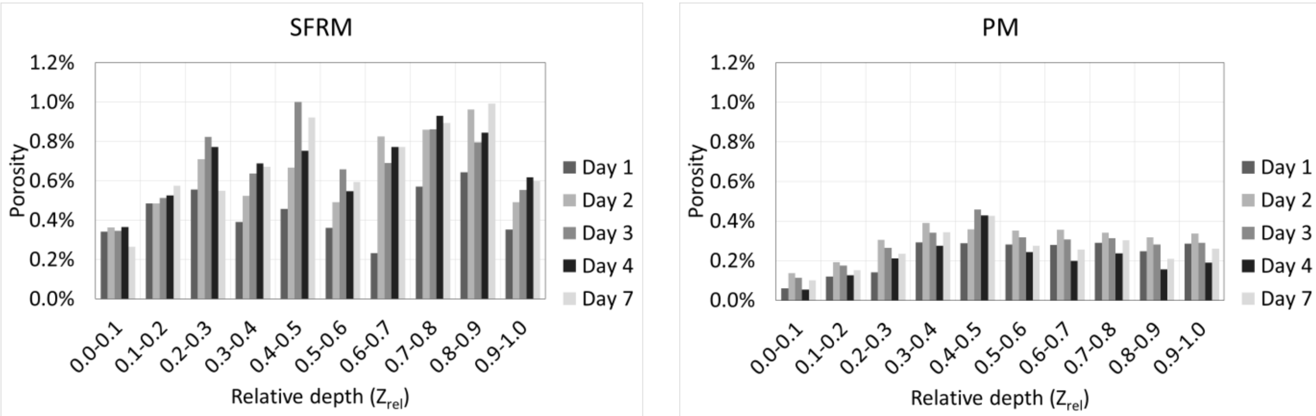

Figure 9: Change of porosity by depth and by age of SFRM specimen (right) and PM specimen (left)

Figure 9 shows some interesting results. First, it may be noted that both SFRM and PM showed a progressive increase of the porosity throughout their depth. The lowest porosity can be observed in the first two tenths of the specimens.

Second, Figure 9 reveals that the SFRM showed, in general, a progressive increase in porosity over time throughout its depth. This tendency was not observed in the first three tenths and was not evident in the PM specimens where the porosity remained almost constant over time in all cases.

Using the data on porosity over time, the line of the results at each depth was fitted to its slope. This value represents the average value of the porosity variation speed over the first 7 days. Figure 10 shows the change of this parameter throughout the depth for both mixtures.

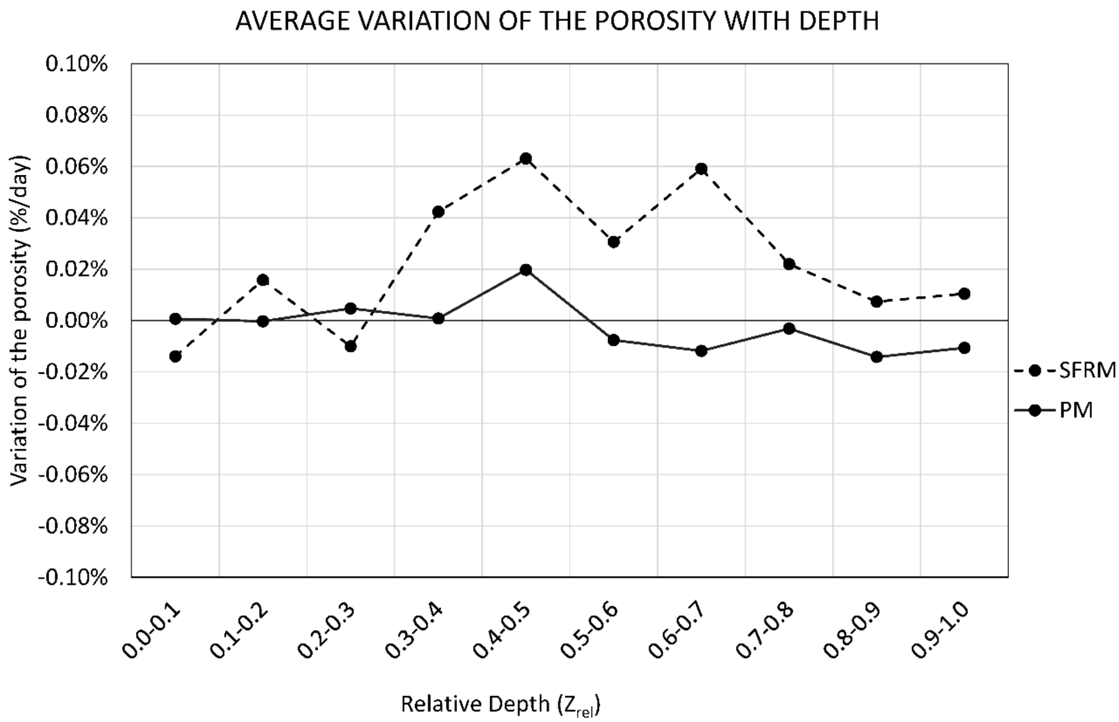

Figure 10: Change of the porosity variation speed along the depth

Figure 10 confirms the findings observed in Figure 9. In general, SFRM showed a positive variation of the porosity over time, while PM showed no relevant changes, i.e., it remained at around zero.

The two opposite mechanisms previously explained can be used to explain these findings. Inside the specimen, i.e., not close to the free surface, the loss of water was mainly due to its consumption during the cement hydration process. In this case, the progressive reduction of free water and, in consequence, the progressive appearance of voids was strongly related to the properties of the cement matrix and its gain in internal stiffness. The water is mostly used to build mortar matrix and, in consequence, to increase the mortar stiffness. Moreover, both phenomena occurred simultaneously, i.e., the loss of water occurred simultaneously with the gains in cement paste stiffness. At the early age, the mortar stiffness is low but most of the voids are full of water (especially the smallest voids), so they are stable. Over time, the voids are emptied but the mortar stiffness increases, so they tend to be stable. In case of the SFRM, the fibers provided extra stiffness to the cement matrix, which prevented the voids from collapsing. On the contrary, the lesser stiffness of the PM cement matrix meant that the voids collapsed with greater frequency.

In contrast, the loss of water close to the free surface was mainly due to evaporation. This phenomenon was unrelated to the properties of the cement matrix and its gain in internal stiffness; moreover, the loss of water happened faster than the gain in cement-paste stiffness. The water is only partially used to build mortar matrix. In consequence, the risk of collapsing voids increased. At the early age, the mortar stiffness is low but most of the voids are full of water (especially the smallest voids), so they are stable. Over time, the voids are emptied and the mortar stiffness does not increase enough, so they tend to be unstable. In this case, the evaporation was relevant and a significant percentage of the specimens were affected by collapse (around 30% of the whole depth), as the specimens were held in an atmospherically controlled room, where they remained at 20ºC and 60% humidity,

In case of the SFRM, the average porosity variation speed was, approximately, 0.02%/day. On the contrary, in case of the PM, the average porosity variation speed was, approximately, 0.00%/day.

In all cases, the specimens showed a slight different behavior around mid-height (i.e., at a relative depth of, approximately, 0.5), because the molds were cast in two parts and showed a higher amount of entrapped air at this height.

3.3 Porosity and porosimetric curves

The exact geometry of each individual void was obtained through the use of the DIP software. In particular, two geometrical dimensions were of interest: void volume and length. The latter parameter is defined as the maximum distance between two voxels belonging to the same void.

Using these two data, the pore volume curves and the porosimetric curves can be plotted. A pore volume curve is defined as the graph that correlates the length of the void and the total pore volume of the voids with a length that is equal or less than the latter. In contrast, the porosimetric curve is defined as the graph showing the correlation between the length of the void and the pore volume of the voids with a length equal to or less than the latter. In both cases, these graphs represent the pore size distribution.

Figure 11 shows the pore volume curves of the two mixtures at different ages, while Figure 12 shows the porosimetric curves of both mixtures at different ages. In all cases, the maximum length was limited to 10 mm as the longer pores were residual.

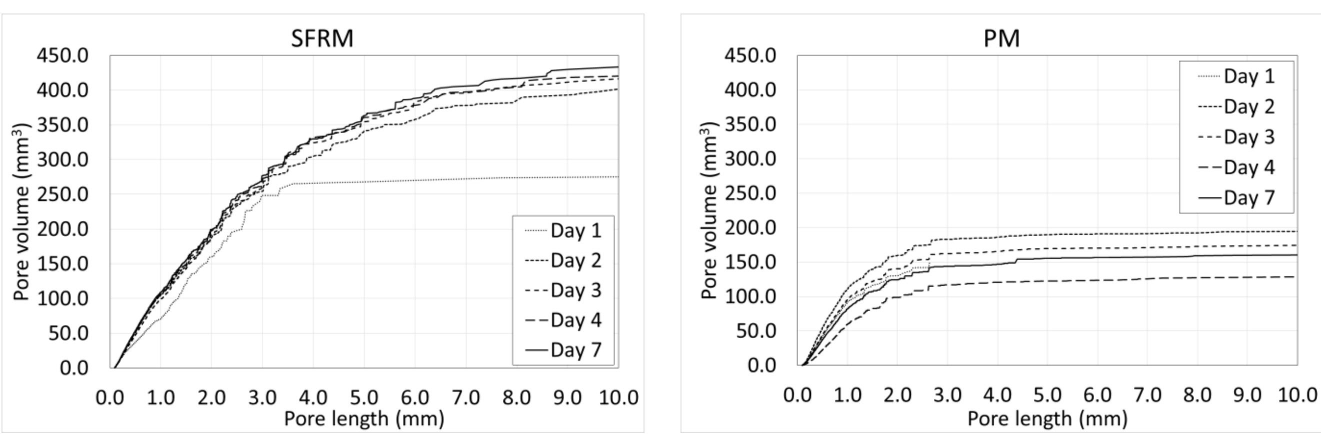

Figure 11: Pore volume curves of SFRM (right) and PM (left)

Figure 11 shows a small change in the pore volume curves by age of mortar and by mixture (SFRM and PM).

In case of SFRM, the pore volume curves measured on the first day were notably lower than the other curves. The latter were almost identical. The different behavior of the first curve can easily be explained, since almost all the voids were full of water so were not considered as voids at that time.

On the contrary, no clear tendency could be observed in PM specimens, suggesting that neither the total pore volume nor the pore size distribution varied with the age of the mortar.

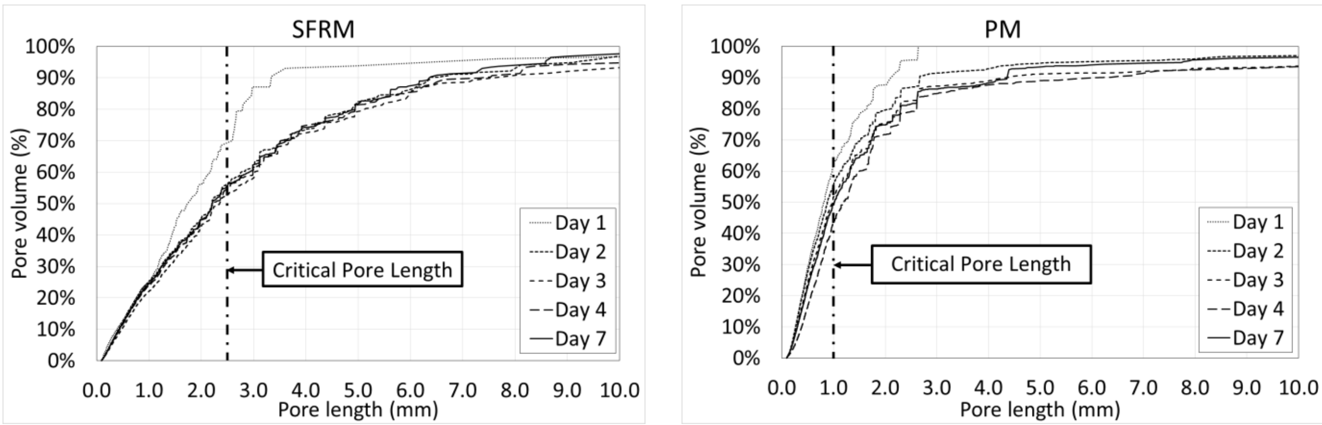

Figure 12: Porosimetric curves of SFRM (right) and PM (left)

In Figure 12, the porosimetric curve of the first day appears, in both cases, above the rest of the curves. This behavior is more clearly observable in SFRM, although it can also be seen in PM specimens. On the remaining days, the porosimetric curves were almost identical, implying no relevant changes in the pore size distribution with the age of the mortar, i.e., the final pore size distribution of the mixture was reached by the second day.

Another interesting observation following the comparison in Figure 12 is that porosimetric curves of the SFRM specimens are lower than those of the PM specimens, implying that the SFRM was capable of retaining greater voids than the PM.

Both the pore volume curves (Figure 11) and the porosimetric curves (Figure 12) are parabolic with a decreasing slope, meaning that the largest amount of air was retained in the smallest voids, measured in both absolute and relative value. As the pore size (pore length) increased, the capacity of retaining air decreased.

Figure 12 also reveals that, in all cases, the curves showed a substantially straight part initially, up to a certain value of pore length, which can be named as “critical pore length”. That is, the critical pore length is defined as the maximum pore length where the slope of the curve pore length – pore volume is constant.

In case of SFRM specimen, the critical pore length shows a value between 2 and 3 mm. Beyond this critical pore length, the slope of the curves started to decrease. In case of PM the critical pore length can be established at 1 mm.

An interesting parameter that can be obtained through the porosimetric curves is the nominal maximum pore size (NMPS) which can be defined, in a similar way to the well-known nominal maximum aggregate size (NMAS), as the pore length corresponding to a cumulative pore volume of 90%. This value is representative of the pore size distribution, as the remaining 10% of the pore volume corresponds to an extremely low number of individual pores (less than 0.05% of the pores, on average). Figure 13 shows the change of the NMPS in both mixtures over time.

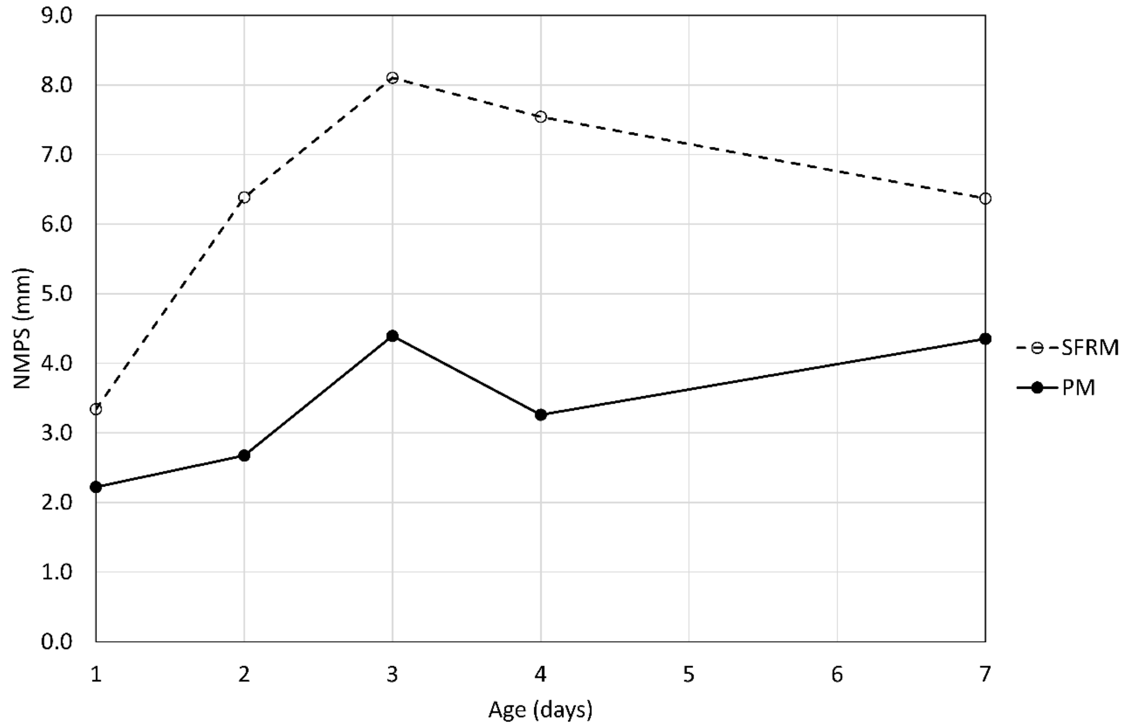

Figure 13: Change of the NMPS by age.

Figure 13 reveals that the NMPS is greater in the SFRM than in the PM specimens at all ages. Hence, the SFRM specimens not only showed a greater pore volume (as can be observed in Figure 8) but also larger voids. In case of the SFRM, there was a relevant increase in the NMPS, up to day 3 after which it started to decrease. However, it can in general be considered that the SFRM specimens showed an increase in NMPS as they aged, which agrees with the results in Figure 12. In case of the PM specimens, the curve also shows an increase in the NMPS up until day 3. Subsequently, a decrease occurred on day 4 and a progressive increase. In general terms, it can be considered that the PM showed an increase in the NMPS with the age of mortar, although less intense than in case of the SFRM.

All the findings shown above can be explained in terms of a greater stiffness of the SFRM fresh cement paste, due to the additional fiber-induced stiffness, with respect to the PM specimens. In case of the SFRM, its fibers added stiffness to the cement paste and stopped the pores from collapsing. The larger the pore, the greater its instability. In consequence, the SFRM specimens were able to withstand a greater percentage of larger pores than the PM specimens.

3.4 Variation of the porosity and porosimetric curves along the depth

The Z coordinate of the voids is known, from which the porosimetric curves throughout the depth may be estimated. The porosimetric curves are shown in Figures 14 and 15 at different depths. In these figures, the considered depth is top to bottom.

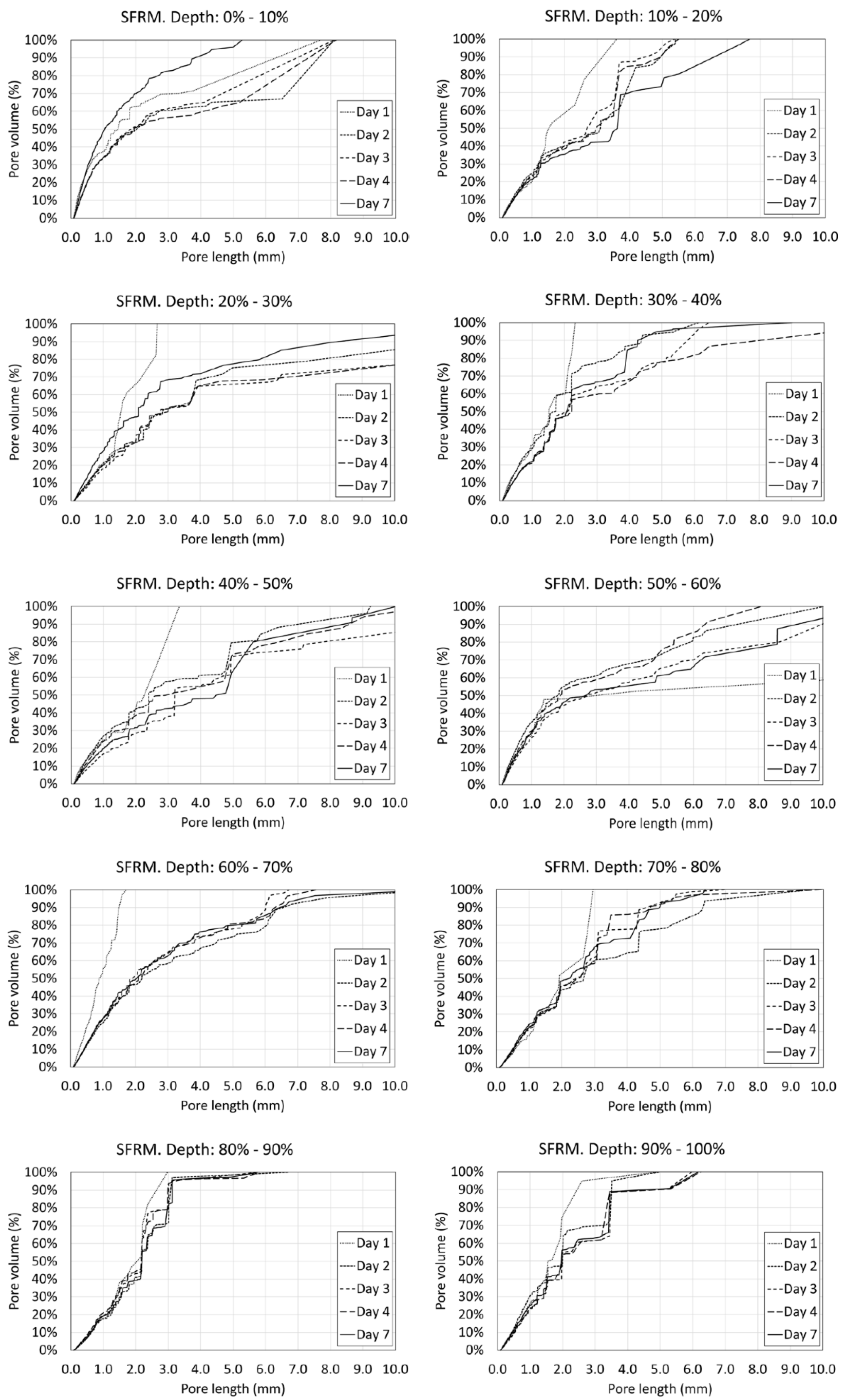

Figure 14: Porosimetric curves of SFRM at different age and throughout the depth.

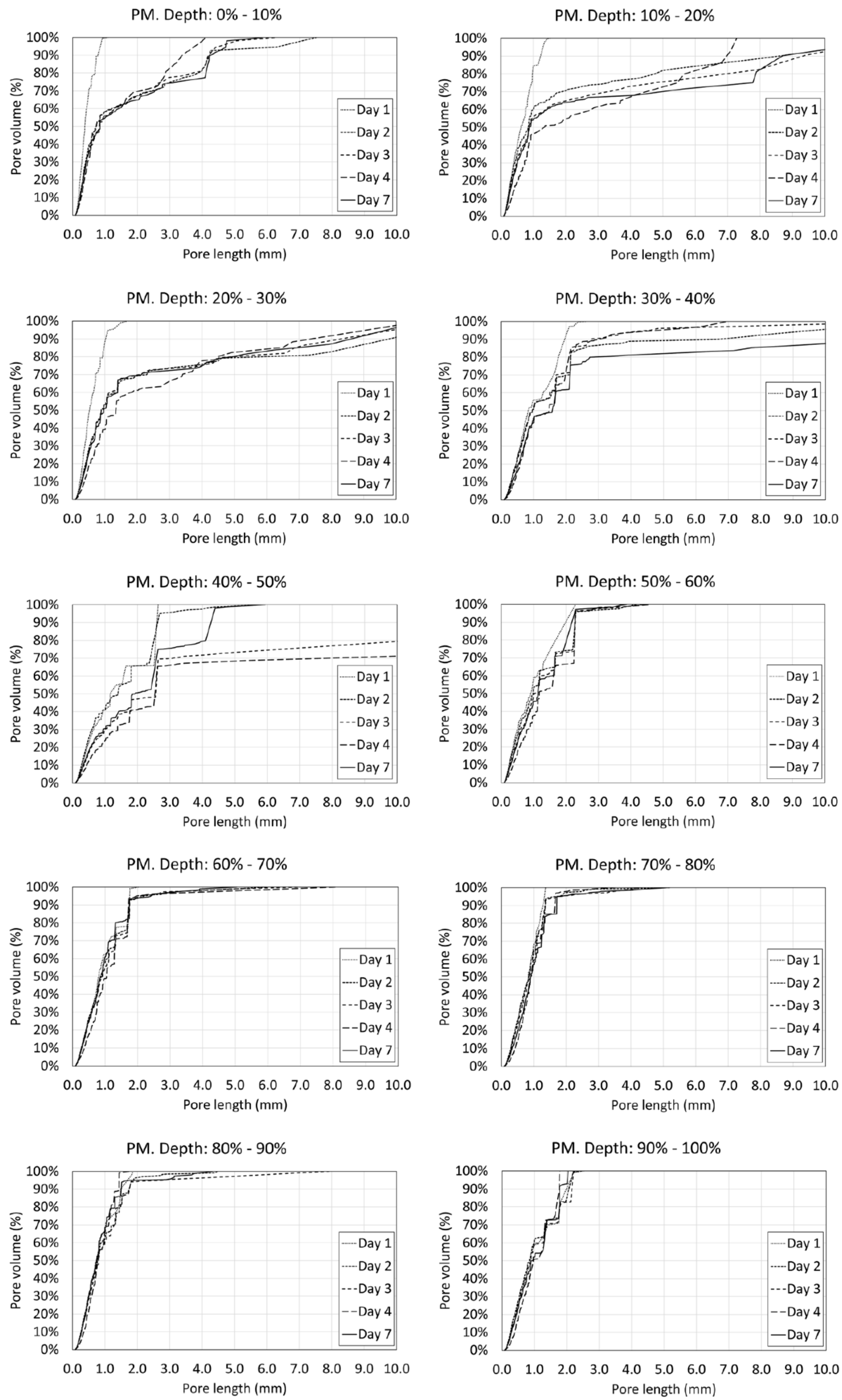

Figure 15: Porosimetric curves of PM at different age and throughout the depth.

Figures 14 and 15 reveal, first of all, that voids are not uniformly distributed throughout the depth. The distance to the free surface, where loss of water occurred, has a strong influence on the pore size distribution.

In both mixtures, the curves for the first day can be seen to show a different behavior from the other days. This behavior can be observed at all the depths, because the day 1 voids are, in general, full of water and are neither detected nor identified by CT-Scanning.

In case of the SFRM, the upper part of the mixture showed a relevant change of the porosimetric curve with the age of mortar. This variation is explained by the more intense evaporation activity in this area, close to the free surface, which significantly affects the porosimetric curves. In the deepest region of the specimens, far from the free surface, the variation is reduced beyond day 4, when the porosimetric curves started to be almost identical.

Something similar was observed at mid-height of the specimens: a relevant change of the porosimetric curves with the age of mortar, due to the molds that were filled in two parts, creating a small horizontal joint in the region, with a relevant amount of entrapped air.

In general, all the porosimetric curves showed a first straight part with high slope. This first part went from zero to a certain critical pore length. Beyond the critical pore length, the slope of the curve was significantly lower. The critical pore length varied with the depth and the overall tendency was for the critical pore length to increase with the depth. However, that value was, in general, between 2 and 4 mm. It could also be observed that the critical pore length referred to a cumulative pore volume that increased with the depth, i.e., the first straight part of the curves reached a higher cumulative pore volume with depth: as the depth increased, the percentage of larger pores also decreased. A behavior explained by the hydrostatic pressure of the fresh mortar that increased with the depth. The smallest voids were able to withstand the higher hydrostatic pressure better; beyond the critical pore volume the voids tended to collapse, breaking up into smaller voids.

In case of the PM, a relevant temporary variation around the mid-height of the specimens was observed. Except for the first day (where many voids are filled with free water and undetectable in the CT-Scan), the tendency is towards a progressive reduction of the greater pores.

In a similar way to the SFRM specimens, all the PM curves were substantially bi-linear. The first part was approximately a straight line with a large slope up to a critical pore length. Beyond this value, the slope of the curve decreased drastically. In all cases, the lines of the first part of the curve showed a similar slope. However, the critical pore length varied between 1 and 3 mm with the depth. Hence, the percentage of larger pores decreased with the depth. The explanation is the same as in case of the SFRM: an inverse relation exists between the hydrostatic pressure of fresh mortar and the maximum stable void volume. The voids smaller to this critical volume were stable, but the larger voids tended to collapse, breaking up into smaller voids.

The slope of the curve, directly related with the viscosity and stiffness of the cement paste [45, 47], was significantly steeper than in SFRM. The lesser stiffness of the PM cement paste caused larger voids to become more unstable than in SFRM specimens and tended to collapse, breaking up into smaller voids.

3.5 Shape factor of the voids.

As explained before, using the data provided by the CT-Scan and the DIP software, it is possible to establish the volume and the length of each void. Then, the shape factor of each pore can be obtained, defined as the quotient between the volume of the pore and the volume of the sphere circumscribed to the pore (eq. 1).

$$SF = \frac{V_p}{\frac{1}{6} \cdot \pi \cdot {L_p}^3} \tag{1}$$

where V_p is the pore volume and L_p is the pore length.

Figure 16 shows the histograms of the shape factor of the different mixtures.

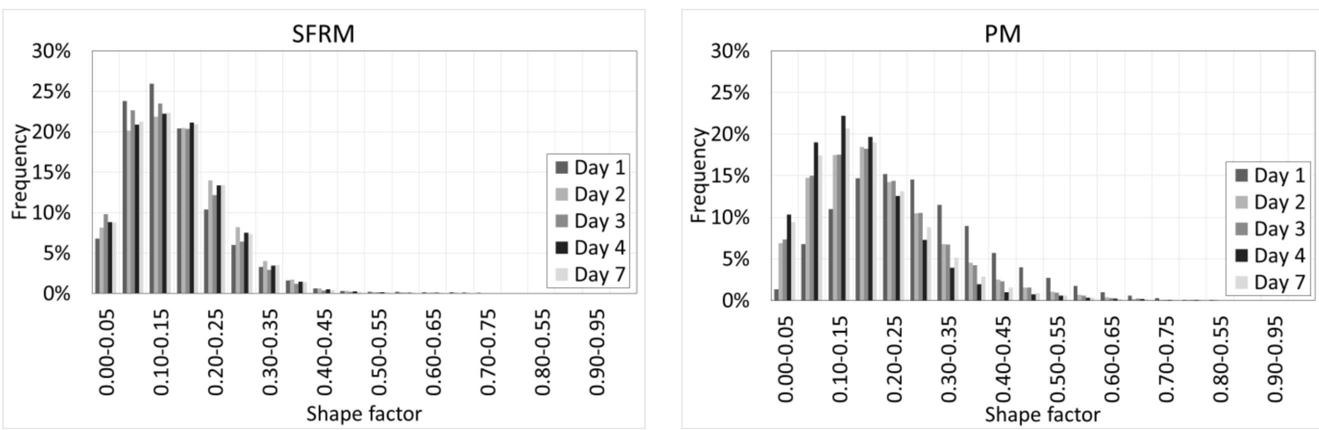

Figure 16: Histogram of the shape factor of SFRM (right) and PM (left)

Some interesting observations can be drawn from Figure 16. First of all, it can be seen that the voids were far from spherical in all cases, as the shape factor was far away from 1. The SFRM specimens showed even smaller shape factors than the PM specimens, with a mode value between 0.10 and 0.15 and over 90% of the voids showed a shape factor below 0.30.

The PM specimens showed higher shape factor values than the SFRM, with a mode value between 0.15 and 0.20 and more than 90% of the voids with a shape factor below 0.40.

These values are explained by the fact that the voids are formed in cement paste components of lesser stiffness and tend to occupy the spaces that are not occupied by the other cement paste components. These spaces tend not to be spherical, but flaky and elongated. In case of the SFRM, the spaces tend to be even flakier and/or more elongated because of the fiber presence. Once again, the fibers modified the pore morphology.

Regarding the variations of the shape factor histogram, it may be seen that, the histograms of the SFRM specimens move toward a larger shape factor as the age of the mortar increases. On the contrary, the PM histograms move toward smaller shape factors as the age of the mortar increases. However, in both cases this variation is not very relevant.

The shape factor showed relevant changes throughout the depth. The shape factor histograms for both mixtures are shown in Figures 17 and 18 at different ages and at different depths.

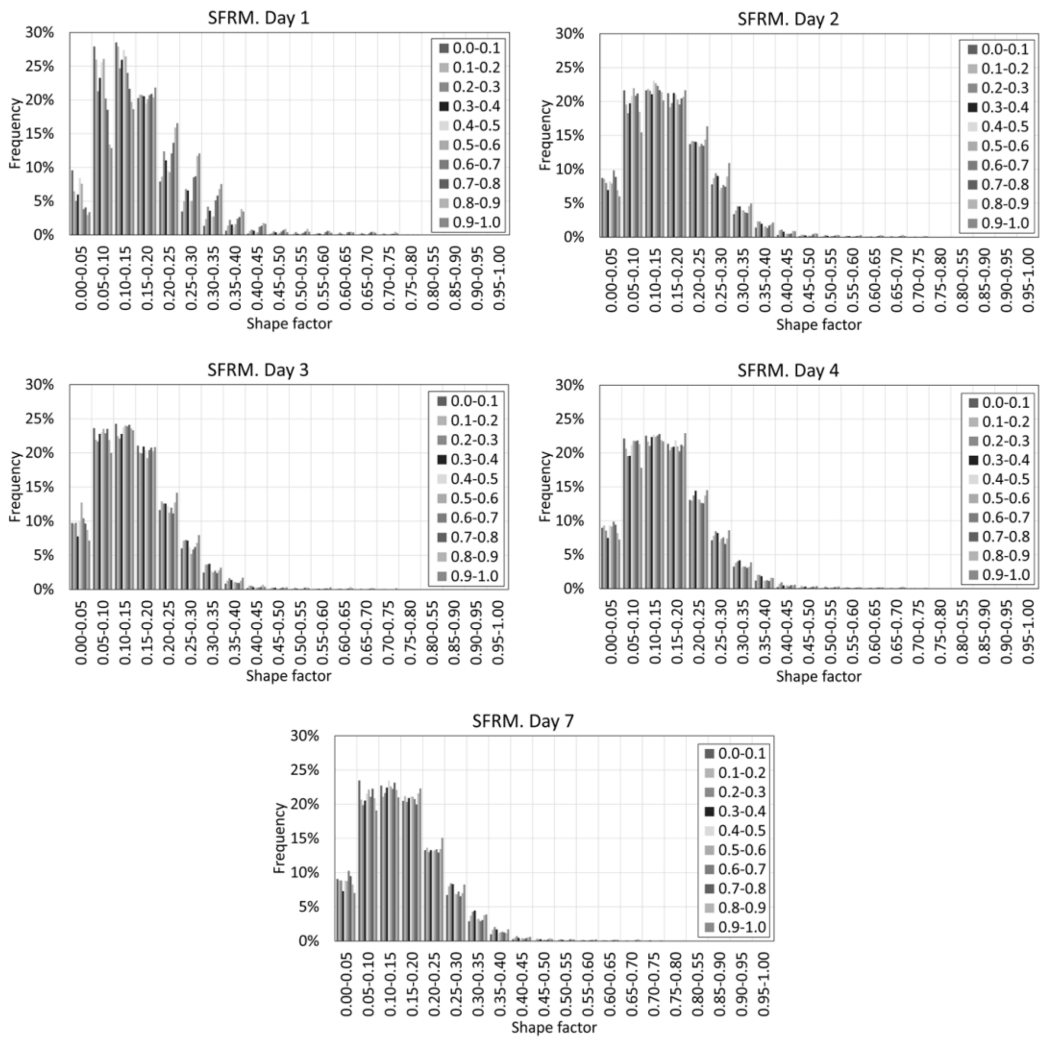

Figure 17: SFRM shape factor histograms by depth and by the age of mortar.

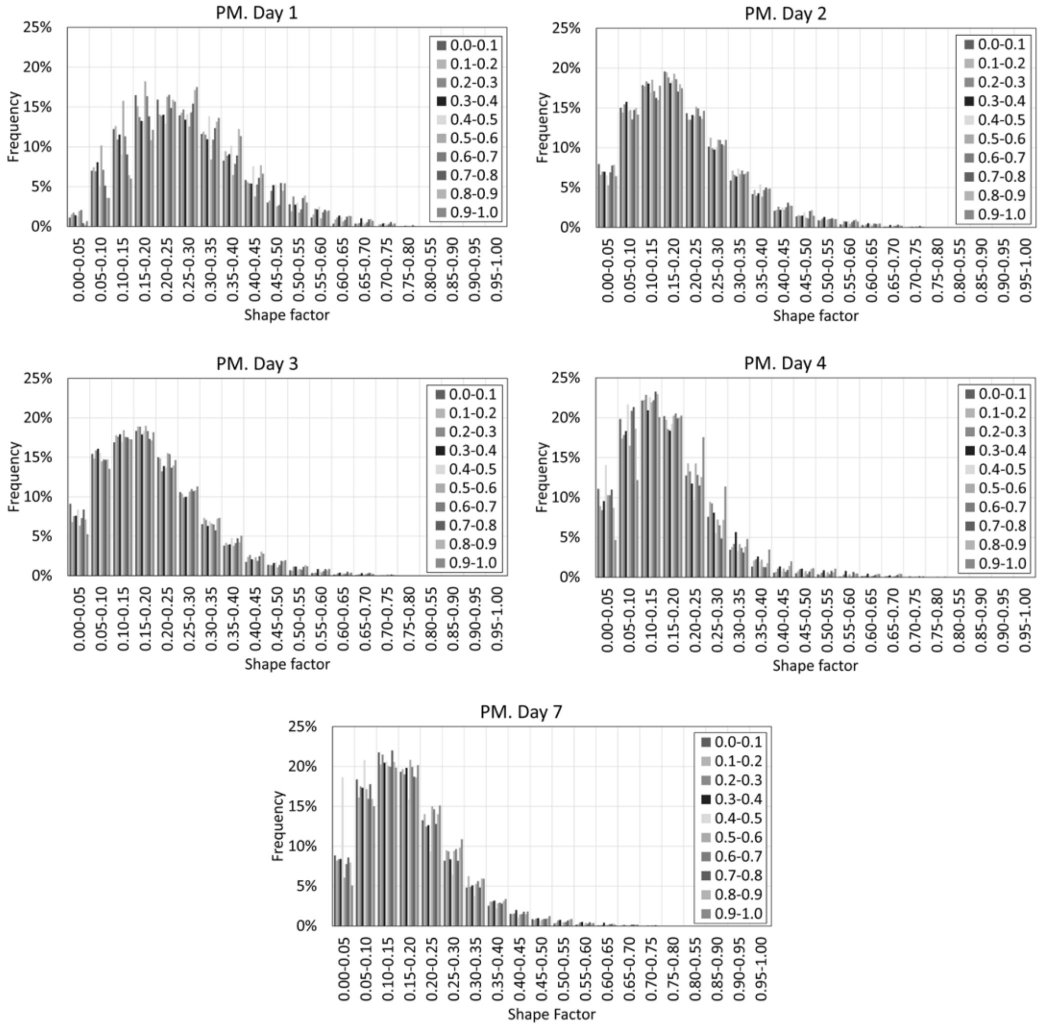

Figure 18: PM shape factor histograms by depth and by the age of mortar.

In Figures 17 and 18, day 1 shows a slightly different behavior in both cases. In case of the SFRM, the shape factor histogram for day 1 is positioned slightly to the left, i.e., a smaller shape factor. This smaller size implies that the voids show small shape factors at very early ages and then increase with the age of the mortar. In case of the PM, the difference between the shape factor histogram for day 1 and the other days was more notable and in an opposite direction, i.e., the shape factor histogram for day 1 is positioned slightly to the right, i.e., a higher shape factor. Hence, at very early ages the voids show higher shape factors and then decrease with the age of the mortar.

Regarding the variation of the shape factor by depth it can be seen that this change was very small in SFRM specimens. Day 1 deserves a special mention, where it is clearly observed that the shape factor histogram moves toward the right as the depth increases, i.e., the shape factor increases with the depth; a variation that is hardly observable over the other days.

In case of the PM specimens, a small movement of the shape factor histograms toward the right was observed, i.e., a slight reduction of the percentage of voids with the smallest shape factor and, in consequence, a slight increase of the percentage of voids with higher shape factors. This increase was due to the hydrostatic pressure of fresh cement paste, which promoted the creation of voids with a more stable geometry, i.e., more spherical.

However, in PM specimens, the change of the shape factor histograms tended to be a slightly chaotic with the age of the mortar. The collapse of the pores, as explained previously, was due to the lesser stiffness of the fresh cement past, which changed the shapes of the voids over time. These changes were clearly observed on day 4, where there was a relevant increase in the percentage of pores with smaller shape factors.

4. CONCLUSIONS

The change of the internal pore morphology of two different mixtures has been analyzed throughout the first week of curing, using a CT-Scan and DIP software. Both mixtures showed the same components and dosage of the cement matrix and the only difference between them was that the SFRM mixture incorporated 0.1% by volume of steel fibers, while the PM mixture included no fibers.

The pore morphology was measured during the first week of curing, when most of the variations within the mortar matrix are expected to occur, at 5 different ages, i.e., 1, 2, 3, 4 and 7 days.

Some interesting conclusions have been obtained. First, it can be noted that the SFRM specimens showed greater porosity than the PM specimens. This difference was observed over all the days under study. The porosity increased with the age of mortar in both cases, although it was more relevant in SFRM specimens.

Most of these observations can be explained by the stiffness of the fresh cement paste. At the beginning of the hardening process almost all the voids are full of water. Over time, the water is consumed and the space occupied initially by water is then filled with air, and the voids appear. There are two water-consumption mechanisms and, in consequence, two ways of creation of voids. The first mechanism is the hydration process, which has a high water-consumption rate affecting the whole specimen. The second mechanism is water evaporation, which only occurs close to the free surface.

With regard to the first phenomenon, there was a strong relation between the creation of voids and the increased stiffness of the fresh cement paste. In case of the SFRM specimens, the extra fiber-induced stiffness permitted the retention of larger voids. In case of the PM specimens, the absence of this extra stiffness meant that the larger voids tended to collapse.

Water loss happened more quickly closer to the free surface and not all of it was used to create the cement paste (because of water evaporation). The consequence was a lower mortar stiffness close to free surface that could only retain smaller voids. Even in case of the SFRM specimens, the fibers provided no extra stiffness in an efficient way.

The porosimetric curves showed two different parts. The first one belonging to the smaller sizes, went from 0 to a critical length. In this part, the curves tended towards a straight line and beyond that critical length, the slope of the curves decreased. The critical length of the SFRM specimens was defined between 2 and 3 mm, while the critical length was around 1 mm for the PM specimens. This behavior was observed throughout the depth, although the value of the critical length varied slightly with the depth, especially in SFRM specimens.

The critical length is, again, closely related to the stiffness of the fresh cement paste and its capacity to develop voids. In case of the SFRM specimens, the extra fiber-induced stiffness permits higher retention of mortar pores of up to 2-to-3 mm in length. Beyond this value, the pores became more instable and tended to collapse, breaking down into smaller ones. In case of the PM specimens, the lower stiffness of the cement paste and its capacity to retain pores was reduced; voids beyond 1 mm length were only retained with difficultly and tended to collapse.

Some interesting conclusions have also been drawn from the shape factor histograms. First of all, it can be noted that rather than spherical, the pores were flaky and elongated. The shape factor of the SFRM specimens due to the presence of fibers was smaller than the PM shape factor. In case of the SFRM, the shape factor increased with both the age and the depth of the mortar. On the contrary, in case of the PM, the shape factor decreased with the age of the mortar, although it increased with the depth. However, the change was in all cases less relevant.

It has therefore been demonstrated in this study that fibers modify several aspects of pore morphology: they increase mortar porosity, increase mortar pore size and reduce the shape factor, among other effects. This should be used in the design of mortar mixtures, especially when a certain of entrained/entrapped air is required.

5. ACKNOWLEDGEMENTS

The authors are grateful for the financial support from the Ministerio de Economía y Competitividad, BIA2015-68678-C2-R, Spain.

REFERENCES

[1]. Mehdipour, I..; Khayat, K.H (2018). “Understanding the role of particle packing characteristics in rheophysical properties of cementitious suspensions: A literature review”. Construction and Building Materials, v 161, pp. 340-353.

[2]. Lazniewska-Piekarczyk, B. (2012). "The influence of selected new generation admixtures on the workability, air-voids parameters and frost-resistance of self compacting concrete". Construction and Building Materials, v 31, 310-319.

[3]. Li, Z. (2007). "State of workability design technology for fresh concrete in Japan". Cement and Concrete Research, v 37, pp. 1308-1320.

[4]. Kim, H.K.; Jeon, J.H.; Lee, H.K. (2012). "Workability, and mechanical, acoustic and thermal properties of lightweight aggregate concrete with a high volume of entrained air". Construction and Building Materials, v 29, pp. 193-200.

[5]. Chandrappa, A.K.; Biligiri, K.P. (2018). "Pore Structure Characterization of Pervious Concrete Using X-Ray Microcomputed Tomography". Journal of Materials in Civil Engineering, v 30(6): 04018108, 1 to 11.

[6]. Liu, B.; Luo, G.; Xie, Y. (2018). "Effect of curing conditions on the permeability of concrete with high volume mineral admixtures". Construction and Building Materials, v 167, pp. 359-371.

[7]. Akand, L.; Yang, M.; Gao, Z. (2016). "Characterization of pervious concrete through image based micromechanical modeling". Construction and Building Materials, v 114, pp. 547-555.

[8]. Ley, M.T.; Welcher, D.; Peery, J.; Khatibmasjedi, S.; LeFlore, J. (2017). "Determining the air-void distribution in fresh concrete with the Sequential Air Method". Construction and Building Materials, v 150, pp. 723-737.

[9]. Jin, S.; Zhang, J.; Huang, B. (2013). "Fractal analysis of effect of air void on freeze-thaw resistance of concrete". Construction and Building Materials, v 47, pp. 126-130.

[10]. Narayanan, N.; Ramamurthy, K. (2000). "Structure and properties of aerated concrete: a review". Cement & Concrete Composites, v 22, pp. 321-329.

[11]. Vicente, M.A.; González, D.C.; Mínguez, J.; Tarifa, M.A.; Ruiz, G. (2018a). "Influence of the pore morphology of high strength concrete on its fatigue life". International Journal of Fatigue, v 112; pp. 106-116.

[12]. Vicente, M.A.; Ruiz, G.; González, D.C.; Mínguez, J.; Tarifa, M.; Zhang, X. (2018b). "CT-Scan study of crack patterns of fiber-reinforced concrete loaded monotonically and under low-cycle fatigue". International Journal of Fatigue, v. 114, pp. 138-147.

[13]. Chen, X.; Wu, S.; Zhou, J. (2013). "Influence of porosity on compressive and tensile strength of concrete mortar". Construction and Building Materials, v 40, pp. 869-874.

[14]. Chen, X.; Xu, L.; Wu, S. (2016). "Influence of pore structure on mechanical behavior of concrete under high strain rates". Journal of Materials in Civil Engineering, v 28(2): 04015110, 1 to 8.

[15]. Chen, Y.; Wang, K.; Wang, X.; Zhou, W. (2013). “Strength, fracture and fatigue of previous concrete”. Construction and Building Materials, v 42, pp. 97-104.

[16]. Zeng, Q.; Li, K.; Fen-Chong, T.; Dangla, P. (2012). “Pore structure characterization of cement pastes blended with high-volume fly-ash”. Cement and Concrete Research, v 42(1), pp. 194-204.

[17]. Herrmann, H.; Pastorelli, E.; Kallonen, A.; Suuronen, J.P. (2016). “Methods for fibre orientation analysis of X-ray tomography images of steel fibre reinforced concrete (SFRC)”. Journal of Materials Science, v 51(8), pp. 3772-3783.

[18]. Vicente, M.A.; González, D.C.; Mínguez, J. (2014). “Determination of dominant fibre orientations in fibre-reinforced high strength concrete elements based on computed tomography scans”. Nondestructive Testing and Evaluation, v 29(2), pp. 164–182.

[19]. Lu, H.; Peterson, K.; Chernoloz, O. (2018). “Measurement of entrained air-void parameters in Portland cement concrete using micro X-ray computed tomography”. International Journal of Pavement Engineering, v 19(2), pp. 109-121.

[20]. Wang, Y-S.; Dai, J-G. (2017). “X-ray computed tomography for pore-related characterization and simulation of cement mortar matrix”. NDT & E International, v 86, pp. 28–35.

[21]. Moradian, M.; Hu, Q.; Aboustait, M.; Ley, M.T.; Hanan, J.C.; Xiao, X.; Scherer, G.W.; Zhang, Z. (2017). “Direct observation of void evolution during cement hydration”. Materials and Design, v 136, pp: 137–149.

[22]. Lu, H.; Alymov, E.; Shah, S.; Peterson, K. (2017). “Measurement of air void system in lightweight concrete by X-ray computed tomography”. Construction and Building Materials, v 152, pp. 467–483.

[23]. Vicente, M.A.; Mínguez, J.; González, D.C. (2017). “The use of computed tomography to explore the microstructure of materials in civil engineering: from rocks to concrete”. In: Halefoglu Ahmet Mesrur, editor. Computed tomography - advanced applications. InTech.

[24]. Yuan, J.; Liu, Y.; Li, H.; Yang, C. (2016). “Experimental investigation of the variation of concrete pores under the action of freeze-thaw cycles”. Procedia Engineering, v 161, pp. 583-588.

[25]. Ponikiewski, T.; Katzer, J.; Bugdol, M.; Rudzki, M. (2014). “Determination of 3D porosity in steel fibre reinforced SCC beams using X-ray computed tomography”. Construction and Building Materials, v 68, pp. 333-340.

[26]. Kim, K.Y.; Yun, T.S.; Choo, J.; Kang, D.H.; Shin, H.S. (2012). “Determination of air-void parameters of hardened cement-based materials using X-ray computed tomography”. Construction and Building Materials, v 37, pp. 93-101.

[27]. Zia, A.; Ali, M. (2017). “Behavior of fiber reinforced concrete for controlling the rate of cracking in canal-lining. Construction and Building Materials, v 155, pp. 726-739.

[28]. Ferrara, L.; Park, Y-D.; Shah, S.P. (2007). "A method for mix-design of fiber-reinforced self-compacting concrete". Cement and Concrete Research, v 37, pp. 957-971.

[29]. Gonzalez, D.C.; Moradillo, R.; Mínguez, J.; Martínez, J.A.; Vicente, M.A. (2018). "Postcracking residual strengths of fiber-reinforced high-performance concrete after cyclic loading". Structural Concrete, v 19(2), pp. 340-351.

[30]. Parvez, A.; Foster, S.J. (2015). "Fatigue Behavior of Steel-Fiber-Reinforced Concrete Beams". Journal of Structural Engineering, v 141(4): 04014117: 1 to 8.

[31]. González, D.C.; Vicente, M.A.; Ahmad, S. (2015). "Effect of cyclic loading on the residual tensile strength of steel fiber–reinforced high-strength concrete". Journal of Materials in Civil Engineering, v 27(9): 04014241: 1 to 8.

[32]. Minguez, J.; González, D.C.; Vicente, M.A. (2018). "Fiber geometrical parameters of fiber-reinforced high strength concrete and their influence on the residual post-peak flexural tensile strength". Construction and Building Materials, v 168, pp. 906-922.

[33]. Bischoff, P.H. (2003). "Tension stiffening and cracking of steel fiber-reinforced concrete". Journal of Materials in Civil Engineering, v 15(2), pp. 174-182.

[34]. Al Rikabi, F.T.; Sargand, S.M.; Khoury, I.; Hussein, H.H. (2018). "Material properties of synthetic fiber–reinforced concrete under freeze-thaw conditions". Journal of Materials in Civil Engineering, v 30(6): 04018090, 1 to 13.

[35]. Niu, D.; Jiang, L.; Bai, M.; Miao, Y. (2013). "Study of the performance of steel fiber reinforced concrete to water and salt freezing condition". Materials and Design, v 44, pp. 267-273.

[36]. Ding, X.; Li, C.; Han, B.; Lu, Y.; Zhao, S. (2018). "Effects of different deformed steel-fibers on preparation and fundamental properties of self-compacting SFRC". Construction and Building Materials, v. 168, pp. 471-481.

[37]. Meng, W.; Khayat, K.H. (2018). "Effect of hybrid fibers on fresh properties, mechanical properties and autogenous shrinkage of cos-effective UHPC". Journal of Materials in Civil Engineering, v 30(4): 04018030, 1 to 8.

[38]. Malaszkiewicz, D. (2017). "Influence of polymer fibers on rheological properties of cement mortars". Open Engineering, v. 7, pp. 228-236.

[39]. Mehdipour, I.; Ali Libre, N.; Shekarchi, M.; Khanjani, M. (2013). "Effect of workability characteristics on the hardened performance of FRSCCMs". Construction and Building Materials, v. 40, pp. 611-621.

[40]. Grünewald, S.; Walraven, J.C. (2001). "Parameter-study on the influence of steel fibers and coarse aggregate content on the fresh properties of self-compacting concrete". Cement and Concrete Research, v. 31, pp. 1793-1798.

[41]. Roig-Flores, M.; Simicevic, F.; Maricic, A.; Serna, P.; Horvat, M. (2018). "Interfacial transition zone in mature fiber-reinforced concretes". ACI Materials Journal, No. 115-M56, pp. 623-632.

[42]. Xu, L.; Deng, F.; Chi, Y. (2017). “Nano-mechanical behavior of the interfacial transition zone between stee-polypropylene fiber and cement paste”. Construction and Building Materials, v. 145, pp. 619-638.

[43]. Wang, H.X.; Jacobsen, S.; He, J.Y.; Zhang, Z.L.; Lee, S.F.; Lein, H.L. (2009). “Application of nanoindentation testing to study of the interfacial zone in steel fiber reinforced mortar”. Cement and Concrete Research, v. 39, pp. 701-715.

[44]. British Standards Institution. (2016). “Methods of testing cement. Determination of strength.” EN 196-1:2016, London.

[45]. British Standards Institution. (1999). “Methods of test for mortar for masonry. Determination of consistence of fresh mortar (by flow table).” EN 1015-3:1999, London.

[46]. Domingues A.; Ceccato M.R. (2015). “Workability Analysis of Steel Fiber Reinforced Concrete Using Slump and Ve-Be Test”. Materials Reseach, v 18(6), pp. 1284-1290.

[47]. Mazaheripour, H.; Ghambarpour, S.; Mirmoradi, S.H.; Hosseinpour, I. (2011). “The effect of polypropylene fibers on the properties of fresh and hardened lightweight self-compacting concrete”. Construction and Building Materials, vol. 25, pp. 351-358.